On self-similarity properties of isotropic turbulence in numerical simulations of the compressible Euler equations

By WOLFRAM SCHMIDT[1,2], W. HILLEBRANDT[1] AND J. C. NIEMEYER[2]

[1]Max-Planck-Institut für Astrophysik, Garching, Germany
[2]Universität Würzburg, Würzburg, Germany

(Received June 2004)

We present numerical calculations of the parameters C_ν, C_ϵ and C_κ associated with the common closures for turbulence production, dissipation and diffusion. In the case of homogeneous and isotropic turbulence, these parameters are expected to be statistically scale-invariant within the inertial subrange. In order to scrutinise this conjecture, we utilised a generalisation of the Germano filtering formalism, which is applicable to compressible flows as well. The filtering of data obtained from three-dimensional direct numerical simulations of forced isotropic turbulence with Mach numbers in the range $\sim 0.1 \ldots 1$ then yielded values of the closure parameters associated with different length scales. The results indicate that the closure parameters are nearly universal for subsonic or moderately transonic flows, although the resolution of 432^3 grid cells in our simulations is not quite sufficient to clearly establish scale invariance. In addition, it was found that the customary assumption of a kinetic Prandtl number of about unity for the gradient-diffusion closure is flawed due to the misalignment between turbulent flux and the gradient of the turbulence energy. Nevertheless, sound correlation can be achieved if the flux magnitude rather than the flux vector is locally matched. This conclusion is particularly useful for the family of subgrid scale models based on the turbulence energy equation. Furthermore, the parameter of production C_ν was computed in the fashion of dynamical procedures. Thereby, superior agreement between modelled and explicitly evaluated turbulence stresses in comparison to the eddy-viscosity closure with constant C_ν was verified.

1. Introduction

The notion of self-similarity plays an important role in the numerical computation of turbulent flows, particularly, in large-eddy simulations (LES; see Sagaut, 2001). The key idea is that the large-scale features of the flow are shaped by the action of external forces and the imposed boundary conditions, whereas structures on smaller scales are mostly determined by the non-linear transfer of kinetic energy through a cascade of vortices. The dynamics on the largest scales, which constitute the *energy-containing range*, must be explicitly computed in a LES. On the other hand, turbulent velocity fluctuations on smaller scales, which are contained in the so-called *inertial subrange*, are considered to be statistically self-similar. Usually, this property of inertial-range turbulence is expressed in terms of scale-invariant probability distribution functions associated with structural properties of the flow. It becomes beautifully manifest in the $k^{-5/3}$ power law of Kol-

mogorov's theory. In the context of *closures* for second or higher order moments of the velocity field (and, possibly, other quantities), the associated parameters are expected to become asymptotically scale-invariant, once the cutoff length scale sufficiently penetrates the inertial subrange. If this supposition was validated, it would bear important consequences on the treatment of the unresolved fraction of turbulence in LES, i. e., the problem of subgrid scale (SGS) modelling (see Meneveau & Katz, 2000).

Inspired by the turbulence energy equation model (see Sagaut, 2001, §4.3.2), we attempted to explicitly evaluate the rate of production and dissipation, respectively, as well as turbulent diffusion in consecutive bands of wave numbers, using data obtained from numerical simulations of forced isotropic turbulence. The dissipation of kinetic energy on the smallest resolved scales in these simulations is entirely due to the implicit viscosity produced by the numerical scheme. The physical viscosity of the fluid is negligible. From structural properties of the flow on larger scales, which appear to be fairly independent of the details of dissipation, we were able to compute the parameters C_ν and C_κ, stemming from the eddy-viscosity and the gradient-diffusion closure, respectively. For the rate of dissipation, we invoked the hypothesis of local equilibrium and computed the parameter C_ϵ associated with the simple dimensional closure. Furthermore, the correlation between modelled and explicitly calculated quantities was investigated. The numerical simulations which provided the fundamental data are briefly outlined in §2. The underlying formalism of filtered quantities is introduced in §3. The following §4, §5 and §6 cover the discussion of various results for the closure parameters and comparisons between the corresponding modelled and actual quantities. In the conclusion, the question whether we can indeed speak of self-similarity properties inferred form simulation data is posed. The analysis presented in this paper points towards a positive answer. However, more computing power in order to achieve higher resolution would be desirable. This becomes particularly clear from samples of the turbulence energy spectrum function discussed in §2. In particular, the spectra display the notorious *bottleneck effect*, which is a deviation from inertial-range scaling on length scales close to the cutoff spoils the full visibility of self-similarity to some extent (see Dobler, Haugen, Yousef & Brandenburg, 2003).

2. Forced Isotropic Turbulence

In order to produce numerical realisations of isotropic turbulence, we computed the flow of a compressible fluid set into motion by a random force field in a cubic domain subject to periodic boundary conditions. In the case of statistically isotropic and stationary forcing, the outcome is an almost perfect realisation of the mathematical paradigm of homogeneous and isotropic turbulence. Only the imposed periodicity in Cartesian coordinates induces an inherent anisotropy on large scales. The dynamics of the fluid is generally determined by the following set of hydrodynamical conservation laws:

$$\frac{\partial}{\partial t}\rho + \frac{\partial}{\partial x_i}\rho v_i = 0, \tag{2.1}$$

$$\frac{\partial}{\partial t}\rho v_i + \frac{\partial}{\partial x_k}\rho v_i v_k = -\frac{\partial}{\partial x_i}P + \rho f_i + \frac{\partial}{\partial x_k}\sigma_{ik}, \tag{2.2}$$

$$\frac{\partial}{\partial t}E + \frac{\partial}{\partial x_k}E v_k = \rho f_k v_k. \tag{2.3}$$

Energy is injected into the fluid through a mechanical force field $\boldsymbol{f}(\boldsymbol{x}, t)$ called the *driving force* and ultimately dissipated by the microscopic viscosity ν. The corresponding

dissipation tensor σ_{ik} is proportional to the local *rate of strain* of the velocity field:

$$\sigma_{ik} = 2\rho\nu S^*_{ik} \equiv 2\rho\nu \left(S_{ik} - \frac{1}{3} d\delta_{ik} \right), \tag{2.4}$$

where $S_{ik} = \frac{1}{2}(v_{i,k} + v_{k,i})$ and $d = v_{i,i}$. Since mostly velocity fluctuations on the smallest length scales contribute to the strain, microscopic viscous dissipation becomes negligible on larger scales and the fluid dynamics is dominated by non-linear turbulent interactions. At sufficiently high resolution, the cutoff arising from the discretisation in numerical simulations falls into this very range of scales. In consequence, either a subgrid-scale model has to be employed in order to account for the energy transfer from numerically resolved towards unresolved length scales, or a dissipative finite-volume scheme is applied, which properly smoothes the flow on the smallest resolved scales. We chose the latter approach and adopted the *piece-wise parabolic method* (PPM) proposed by Colella & Woodward (1984) for the solution of the hydrodynamical equations. The idea of employing the PPM for direct numerical simulations of turbulent flows was particularly advocated by Sytine, Porter, Woodward, Hodson & Winkler (2000), following systematic convergence tests and comparisons to conventional methods with explicit treatment of the viscosity term. From the numerical point of view, the treatment of the hydrodynamical equations with the PPM corresponds to the limit of zero physical viscosity. In essence, the compressible Euler equations are solved, with the velocity fluctuations on scales smaller than the grid resolution Δ being damped out by numerical dissipation.

The driving force $\boldsymbol{f}(\boldsymbol{x}, t)$ is composed in spectral space, using a three-dimensional generalisation of the scalar *Ornstein-Uhlenbeck process*, as proposed by Eswaran & Pope (1988). The evolution of the Fourier transform $\hat{\boldsymbol{f}}(\boldsymbol{k}, t)$ is given by the following Langevin-type stochastic differential equation:

$$\mathrm{d}\hat{\boldsymbol{f}}(\boldsymbol{k}, t) = -\hat{\boldsymbol{f}}(\boldsymbol{k}, t)\frac{\mathrm{d}t}{T} + F_0 \sum_{jlm} \left(\frac{2\sigma^2(\boldsymbol{k})}{T} \right)^{1/2} \delta(\boldsymbol{k} - \boldsymbol{k}_{jlm}) P_\zeta(\boldsymbol{k}) \cdot \mathrm{d}\boldsymbol{\mathcal{W}}_t, \tag{2.5}$$

The second term on the right hand side accounts for a random diffusion process, which is constructed from a three-component *Wiener process* $\boldsymbol{\mathcal{W}}_t$. The distribution of each component is normal with zero mean and variance $\mathrm{d}t$. The wave vectors $\boldsymbol{k}_{jlm}$ are dual to the position vectors of the cells in the numerical discretisation of the fundamental domain. The symmetric tensor $P_\zeta(\boldsymbol{k})$ is defined by the linear combination of the projection operators perpendicular and parallel to the wave vector. The components of $P_\zeta(\boldsymbol{k})$ can be expressed as

$$(P_{ij})_\zeta(\boldsymbol{k}) = \zeta P^\perp_{ij}(\boldsymbol{k}) + (1-\zeta) P^\parallel_{ij}(\boldsymbol{k}) = \zeta\delta_{ij} + (1-2\zeta)\frac{k_i k_j}{k^2}, \tag{2.6}$$

where the spectral weight ζ determines whether the resulting force field in physical space is purely solenoidal, dilatational or a combination of both. The variance $\sigma^2(\boldsymbol{k})$ specifies the spectrum of the force field. We use a quadratic function, which confines the modes of the force to a narrow interval of wavenumbers, $k \in [0, 2k_0]$. The wave number k_0 determines the *integral length scale* of the flow, $L = 2\pi/k_0$.

The root mean square of the specific driving force is determined by the characteristic magnitude F_0 and the weight ζ:

$$f_{\mathrm{rms}} = \sum_{jlm} \langle \hat{\boldsymbol{f}}_{jlm}(t) \cdot \hat{\boldsymbol{f}}_{jlm}(t) \rangle \simeq (1 - 2\zeta + 3\zeta^2) F_0^2. \tag{2.7}$$

Since F_0 has the physical dimension of acceleration, it can be expressed as the *characteristic velocity* V of the flow divided by the *integral time scale*, which is given by

ζ	V/c_0	t_d/T	t_f/T	$N_{\Delta t}$
1.0	0.084		2.5	5815
1.0	0.42	3.0	8.0	6343
0.75	0.66	5.0	10.0	6351
0.2	1.39	5.0	10.0	3356

TABLE 1. List of simulation parameters: spectral weight ζ of the driving force, characteristic Mach number V/c_0, onset of decay t_d/T, end of simulation t_f/T, number of time steps $N_{\Delta t}$.

the auto-correlation time T of the driving force (2.5). Setting $T = L/V$, we have $F_0 = V/T = LV^2$, and, starting with a homogeneous fluid at rest, the flow is developing towards a fully turbulent steady state within about two integral time scales.

As our work was motivated by the problem of turbulent burning processes in thermonuclear supernovae, we applied the equation of state for a degenerate electron gas in combination with non-degenerate nuclei. This form of matter occurs in compact stellar remnants called white dwarfs (see Hillebrandt & Niemeyer, 2000; Reinecke, 2001). However, once quantities are scaled in terms of characteristic parameters, no major differences to turbulence in, say, an ideal gas are found. The parameters chosen for several particular simulations are listed in table 1. In the simulations with $\zeta = 1$, turbulence was produced by purely solenoidal forcing or "stirring". We chose two different values of the characteristic Mach number V/c_0, where c_0 is the speed of sound in the initially homogeneous fluid at rest. For the lower value, the flow is completely subsonic, whereas for the higher value, it is marginally transonic. Furthermore, we run two simulations with partially dilatational forcing, i. e., the force field has compressive components. In both cases, the velocity of the flow locally exceeds the speed of sound and shocklets are formed. For all simulations, 432^3 grid cells were used and $\alpha = X/L = 3$, where X is the linear size of the fundamental domain. The evolution was computed over an elapse of several integral time scales, such that data dumps corresponding to a statistically stationary state with energy injection balanced by dissipation were obtained. Finally, decay phases were initiated at a certain time t_d by inhibiting the random increments in the evolution of the stochastic force field. Also included in table 1 are the total durations t_f of the simulations in units of the corresponding integral time scales and the required total number of time steps.

Samples of the normalised energy spectrum function $\tilde{E}(\alpha\tilde{k}, t) = (2\pi/\alpha LV^2)E(k, t)$ at representative stages in the production regime, in statistical equilibrium and in the advanced decay regime are plotted in figure 1 (a–c) for the simulation with $\zeta = 0.75$. Due to the discrete nature of the numerical data, the kinetic energy of modes within certain wave number bins was summed up. Also shown are the longitudinal and a transversal fractions of the energy spectrum functions corresponding to, respectively, the compressible and incompressible components of the velocity field. Figure 1 (d–f) shows the corresponding plots of the *compensated* solenoidal spectrum function

$$\Psi^\perp(t) = \left[\frac{\alpha}{2\pi}\langle\tilde{\epsilon}(t)\rangle\right]^{-2/3} (\alpha\tilde{k})^{5/3}\tilde{E}^\perp(t), \tag{2.8}$$

where $\langle\tilde{\epsilon}\rangle = (T/V^2)\langle\epsilon\rangle$ is the normalised mean rate of dissipation. In the inertial subrange, $\Psi_\mathrm{s}(t) \simeq C$ is expected. C is known as the Kolmogorov constant and considered to be more or less universal. From the spectra shown in figure 1, it becomes clear that a resolution of $N = 432$ is just at the brink where an inertial subrange begins to take shape. Even in the quasi-equilibrium state, there is merely a narrow window of wave

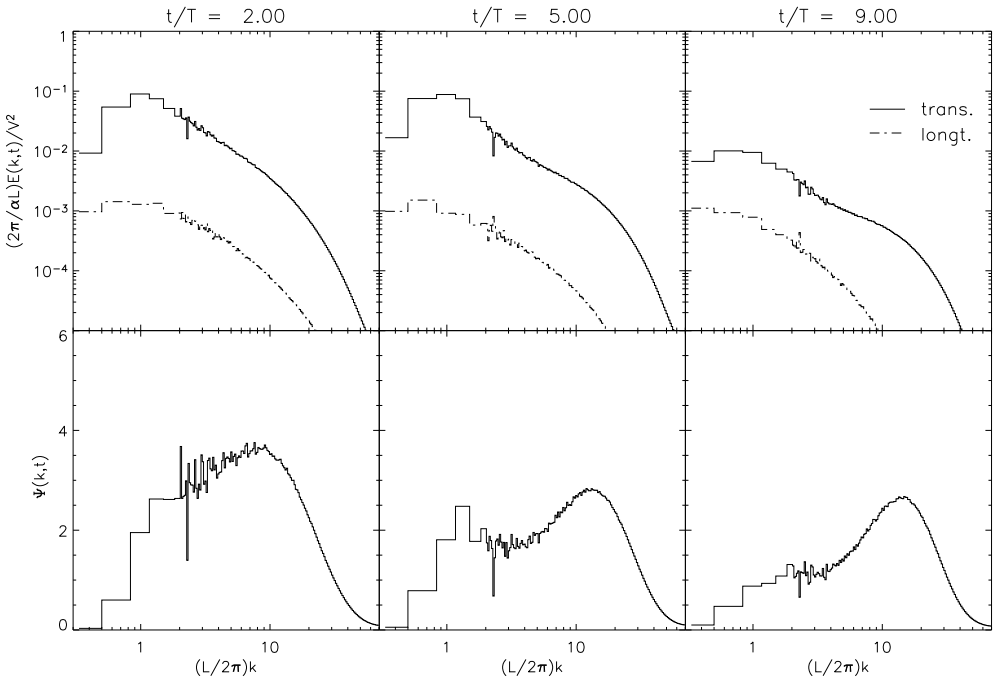

FIGURE 1. Plots of the transversal and longitudinal parts of the turbulence energy spectrum function $\tilde{E}(k,t)$ (a–c: top panels) as well as the compensated transversal spectrum function $\Psi^{\perp}(k,t)$ (d–f: bottom panels) at different times in a simulation of forced isotropic turbulence. The characteristic Mach number is $V/c_0 = 0.66$ and the spectral weight of the driving force $\zeta = 0.75$.

numbers in the vicinity of $\tilde{k} = (L/2\pi)k = 3.0$, in which nearly Kolmogorov scaling with $C \approx 1.7$ is found. In fact, this value of the Kolmogorov constant is comfortably within the range of numerical results reported in the literature (see Yeung & Zhou, 19). Both in figure 1 (e) and 1 (f), there is a pronounced maximum of the compensated spectrum function at $\tilde{k} \approx 15$ corresponding to a flattening of the energy spectrum in comparison to the Kolmogorov law (figures 1 b and 1 c). This so-called *bottleneck effect* was observed in many numerical simulations (see Dobler *et al.*, 2003). At time $\tilde{t} = t/T = 1.5$, on the other hand, small-scale features have only partially developed and the spectrum does not show a bump at higher wave numbers (figures 1 a and 1 d). We will not further discuss the bottleneck effect here, but take it as a genuine feature of our simulations.

3. Hierarchical filtering

In this section we shall elaborate the formal concepts of filters and physical fields smoothed over the associated length scales. The formalism was first introduced by Germano (1992) in the framework of incompressible flows. In the following, *mass-weighted* filtered quantities are defined, which are applicable to compressible flows as well. Remarkably, one of the key results obtained by Germano, the so-called *Germano identity*, carries over to the compressible case without modification. In order to avoid confusion, we will subsequently write the quantities given by the hypothetical exact solution of the dynamical equations in the continuum limit, i. e., for infinite resolution, with the superscript ∞ set on top of the corresponding symbol, whereas the standard symbols

refer to numerically computable quantities. Notwithstanding the deplorable lack of any proof of existence, the former shall be called the *ideal* quantities†. For instance, $\overset{\infty}{\boldsymbol{v}}(\boldsymbol{x},t)$ is identified with the ideal velocity field, i. e., the exact solution of the Navier-Stokes or Euler equation, while it is understood that $\boldsymbol{v}(\boldsymbol{x},t)$ is an approximation to the velocity field, say, an interpolating function to some finite-volume solution.

Since we are mostly concerned with statistically stationary homogeneous turbulence, it is convenient to introduce an infinite series of homogeneous and time-independent filters $\langle\,\rangle_n$. The kernel of the n-th filter is denoted as $G_n(\boldsymbol{x})$. The corresponding *filter operation* on a dynamical quantity $q(\boldsymbol{x},t)$ is defined by

$$q^{(n)}(\boldsymbol{x},t) = \int \mathrm{d}^3x'\, G_n(\boldsymbol{x}')\overset{\infty}{q}(\boldsymbol{x}',t) \tag{3.1}$$

and symbolically written as $q^{(n)} = \langle\overset{\infty}{q}\rangle_n$. In the limit $n\to\infty$, the identity operator is obtained. Here we shall assume that $\langle\,\rangle_n$ is a Gaussian filter with a characteristic length Δ_n and wave number $k_n = \pi/\Delta_n$. The corresponding kernel is given by (see Pope, 2000, §13.2)

$$G_n(\boldsymbol{x}) = \left(\frac{6}{\pi\Delta_n^2}\right)^{3/2} \exp\left(-\frac{6|\boldsymbol{x}|^2}{\Delta_n^2}\right). \tag{3.2}$$

In the following, a series of Gaussian filters with $\Delta_n = L/n$, $n\in\mathbb{N}$, is used, where L is the integral length scale of the flow.

The velocity field $\boldsymbol{v}^{[n]}(\boldsymbol{x},t)$ at the n-th filter level is defined by a *Favre mass-weighted* filter operation:

$$\boldsymbol{v}^{[n]}(\boldsymbol{x},t) = \frac{1}{\rho^{(n)}(\boldsymbol{x},t)} \int \mathrm{d}^3x'\, G_n(\boldsymbol{x}')\overset{\infty}{\rho}(\boldsymbol{x}',t)\overset{\infty}{\boldsymbol{v}}(\boldsymbol{x}',t) \tag{3.3}$$

or, for brevity, $\boldsymbol{v}^{[n]} = \langle\overset{\infty}{\rho}\overset{\infty}{\boldsymbol{v}}\rangle_n/\langle\overset{\infty}{\rho}\rangle_n$. Filtering twice, we set

$$\boldsymbol{v}^{[m][n]}\rho^{(m)(n)} = \langle\rho^{(m)}\boldsymbol{v}^{[m]}\rangle_n = \langle\langle\overset{\infty}{\rho}\overset{\infty}{\boldsymbol{v}}\rangle_m\rangle_n, \tag{3.4}$$

where $\rho^{(m)(n)} = \langle\langle\overset{\infty}{\rho}\rangle_m\rangle_n$. If two filters of characteristic length scales Δ_m and $\Delta_n \gg \Delta_m$ are operating in succession, we have

$$\boldsymbol{v}^{[m][n]}\rho^{(m)(n)} = \langle\rho^{(m)}\boldsymbol{v}^{[m]}\rangle_n \simeq \langle\overset{\infty}{\rho}\overset{\infty}{\boldsymbol{v}}\rangle_n = \boldsymbol{v}^{[n]}\rho^{(n)}. \tag{3.5}$$

The validity of this approximation becomes immediately clear from the product of the kernels of the Gaussian filters in spectral space (see Pope, 2000, §13.2):

$$\hat{G}_m(k)\hat{G}_n(k) = \exp\left[-\frac{k^2(\Delta_m^2+\Delta_n^2)}{24}\right] \simeq \exp\left[-\frac{k^2\Delta_n^2}{24}\right] = \hat{G}_n(k). \tag{3.6}$$

Because the convolution with the filter kernel in physical space corresponds to the multiplication of the Fourier transforms in spectral space, it follows that $\langle\langle q\rangle_m\rangle_n \simeq \langle q\rangle_n$ if $\Delta_n \gg \Delta_m$.

The definition of the filtered velocity at the level n (3.3) is particularly useful, because the equation of motion for the fluid on scales $l \gtrsim \Delta_n$ is given by a *quasi-Navier-Stokes*

† According to Plato's Cave Analogy, the objects we experience in the world are related to their *ideals* like the silhouettes of outside things to someone trapped in a dark cave. In the same way, one can think of a numerically simulated flow as being merely a vague image of the corresponding physical flow or exact mathematical solution of the equations of motion.

equation:

$$\frac{\partial}{\partial t}\,\rho^{(n)}v_i^{[n]} + \frac{\partial}{\partial x_k}\,\rho^{(n)}v_i^{[n]}v_k^{[n]} = -\frac{\partial P^{(n)}}{\partial x_i} + \rho^{(n)}f_i + \frac{\partial}{\partial x_k}(\sigma_{ik}^{(n)} + \tau_{ik}^{[n]}). \tag{3.7}$$

The specific force f_i stirring the fluid is assumed to vary on the largest scales only. This is why the force field is only marginally affected by the filtering operation, and one can set $f_i^{[n]} \simeq f_i$ for $n \gg 1$. In comparison to the *physical* Navier-Stokes equation,

$$\frac{\partial}{\partial t}\,\overset{\infty}{\rho}\overset{\infty}{v_i} + \frac{\partial}{\partial x_k}\,\overset{\infty}{\rho}\overset{\infty}{v_i}\overset{\infty}{v_k} = -\frac{\partial \overset{\infty}{P}}{\partial x_i} + \rho f_i + \frac{\partial}{\partial x_k}\sigma_{ik}, \tag{3.8}$$

the viscous stress tensor $\overset{\infty}{\sigma}_{ik} = 2\overset{\infty}{\rho}\nu\overset{\infty}{S}{}^{*}_{ik}$ for a fluid of microscopic viscosity ν is enhanced by the *turbulence stress tensor* associated with the n-th filter†. The latter is defined by

$$\tau_{ik}^{[n]} = -\langle\overset{\infty}{\rho}\overset{\infty}{v_i}\overset{\infty}{v_k}\rangle_n + \rho^{(n)}v_i^{[n]}v_k^{[n]}. \tag{3.9}$$

In particular, if Δ_n is large compared to the length scale of viscous dissipation, then $\tau_{ik}^{[n]}$ dominates over $\sigma_{ik}^{(n)}$, and (3.7) becomes a *quasi-Euler equation*, in which the microscopic viscosity ν does not appear at all.

For two consecutive filter levels, say, n and $n-1$, there is a simple algebraic relation between the corresponding stress tensors:

$$\tau_{ik}^{[n][n-1]} = \langle\tau_{ik}^{[n]}\rangle_{n-1} + \tau^{[n,n-1]}(v_i^{[n]}, v_k^{[n]}), \tag{3.10}$$

where

$$\begin{aligned}\tau_{ik}^{[n][n-1]} = &-\langle\langle\overset{\infty}{\rho}\overset{\infty}{v_i}\overset{\infty}{v_k}\rangle_n\rangle_{n-1} + \frac{\langle\langle\overset{\infty}{\rho}\overset{\infty}{v_i}\rangle_n\rangle_{n-1}\langle\langle\overset{\infty}{\rho}\overset{\infty}{v_k}\rangle_n\rangle_{n-1}}{\langle\langle\overset{\infty}{\rho}\rangle_n\rangle_{n-1}} = \\ &-\langle\langle\overset{\infty}{\rho}\overset{\infty}{v_i}\overset{\infty}{v_k}\rangle_n\rangle_{n-1} + \rho^{(n)(n-1)}v_i^{[n][n-1]}v_k^{[n][n-1]}.\end{aligned} \tag{3.11}$$

and

$$\tau^{[n,n-1]}(v_i^{[n]}, v_k^{[n]}) = -\langle\rho^{(n)}v_i^{[n]}v_k^{[n]}\rangle_{n-1} + \frac{1}{\langle\rho^{(n)}\rangle_{n-1}}\langle\rho^{(n)}v_i^{[n]}\rangle_{n-1}\langle\rho^{(n)}v_k^{[n]}\rangle_{n-1} \tag{3.12}$$

is the *intermediate* stress tensor at the filter level n associated with the velocity field filtered at the level $n-1$. The above relation was originally formulated by Germano (1992) for incompressible flows. The relation also applies to arbitrary filter levels, m and n, say. In the limit $\Delta_n \gg \Delta_m$, the contribution from $\langle\tau_{ik}^{[m]}\rangle_n$ becomes negligible and

$$\tau_{ik}^{[n]} \simeq \tau_{ik}^{[m][n]} \simeq \tau^{[m,n]}(v_i^{[m]}, v_k^{[m]}), \tag{3.13}$$

i. e., the turbulence stress associated with the scale Δ_n is not sensitive to the flow structure on much smaller scales. The asymptotic limit of the Germano relation is especially useful for the numerical evaluation of turbulence stresses from numerical data.

Utilising the *consistent Germano decomposition* (see Sagaut, 2001, §3.3.2), the turbulence energy associated with length scales $l \lesssim \Delta_n$ is given by the difference between the filtered and the resolved kinetic energy at the filter level n. This particular notion of turbulence energy was introduced by Germano (1992) and is called the *generalised turbulence energy*. At any filter level, the energy is readily defined by the trace of turbulence

† Here the opposite sign as customary in most of the literature is used in order to make τ_{ik} a proper stress tensor, which enters the right-hand side of the equation for the resolved energy with positive sign.

stress tensor:

$$K^{[n]} = \rho^{(n)} k^{[n]} = -\frac{1}{2}\tau_{ii}^{[n]}. \tag{3.14}$$

This definition avoids several difficulties stemming from the mathematical properties of common filter operations, if the turbulence energy is defined in terms of velocity fluctuations relative to the filtered velocity field in the alternative Leonard's decomposition (see Sagaut, 2001, §3.3.1). Contracting the compressible Germano identity (3.10), we obtain the relation

$$K^{[n][n-1]} = \langle K^{[n]} \rangle_{n-1} + K^{[n,n-1]}, \tag{3.15}$$

where

$$K^{[n,n-1]} = -\frac{1}{2}\tau^{[n,n-1]}(v_i^{[n]}, v_i^{[n]}) \tag{3.16}$$

is the intermediate turbulence energy, i. e., the kinetic energy of modes which are concentrated in the spectral band $[\pi/\Delta_{n-1}, \pi/\Delta_n]$. As opposed to the spectral filter, there are no sharp boundaries between adjacent bands associated with Gaussian filters. Nevertheless, the notion of turbulence energy as proposed by Germano is well-defined and unambiguously associates some energy contents with each band of wave numbers.

The scale separation of the energy budget by means of filtering on a characteristic scale Δ_n also yields a conservation law for the turbulence energy $K^{[n]}$. The result is completely analogous to the dynamical equation for SGS turbulence energy and it also entails various closure problems (see Germano, 1992; Sagaut, 2001, §3.3.2). Adopting the standard closures for production, diffusion and dissipation (see Sagaut, 2001, §4.3.2), we obtain the following approximate equation for the time evolution of $K^{[n]}$:

$$\begin{aligned} \frac{\mathrm{D}^{[n]}}{\mathrm{D}t} k^{[n]} - \frac{1}{\rho^{(n)}} \boldsymbol{\nabla} \cdot \left(\rho^{(n)} C_\kappa^{(n)} \Delta_n \sqrt{k^{[n]}} \boldsymbol{\nabla} k^{[n]} \right) = \\ C_\nu^{(n)} \Delta_n \sqrt{k^{[n]}} |S^{*\,[n]}|^2 - \frac{2}{3} k^{[n]} d^{[n]} - C_\epsilon^{(n)} \frac{(k^{[n]})^{3/2}}{\Delta_n}, \end{aligned} \tag{3.17}$$

where $\frac{\mathrm{D}^{[n]}}{\mathrm{D}t} = \frac{\partial}{\partial t} + \boldsymbol{v}^{[n]} \cdot \boldsymbol{\nabla}$ is the Lagrangian time derivative with respect to the filtered velocity field, $S_{ik}^{*\,[n]} = \frac{1}{2}(\partial_k v_i^{[n]} + \partial_i v_k^{[n]}) - \frac{1}{3} d^{[n]} \delta_{ik}$ are the components of the trace-free rate-of-strain tensor and $d^{[n]} = \partial_i v_i^{[n]}$ is the divergence of the velocity field filtered at the level n. Now the question of self-similarity boils down to the scaling-behaviour of the parameters $C_\nu^{(n)}$, $C_\epsilon^{(n)}$ and $C_\kappa^{(n)}$ associated with the different filters in the hierarchy.

4. Kinetic energy transfer

The rate of transfer of kinetic energy from velocity fluctuations on length scales $l > \Delta_n$ towards those on smaller scales is given by the contraction of the turbulence stress tensor and the rate of strain tensor at the level of the n-th filter:

$$\Pi^{(n)} = \tau_{ik}^{[n]} S_{ik}^{[n]}. \tag{4.1}$$

Note that $S_{ik}^{[n]}$ is the symmetrised derivate of the filtered velocity field, i. e., $S_{ik}^{[n]} = \frac{1}{2}(\partial_k v_i^{[n]} + \partial_i v_k^{[n]})$. Since the filter operation involves mass-weighing, differentiation and filtering do *not* commute. The most common closure for the rate of energy transfer is the *eddy-viscosity closure* for the trace-free part of the turbulence stress tensor:

$$\tau_{ik}^{*\,[n]} \mathrel{\hat{=}} 2\rho^{(n)} \nu^{(n)} S_{ik}^{*\,[n]}, \tag{4.2}$$

where $\tau^{*\,[n]}_{ik} = \tau^{[n]}_{ik} - \frac{1}{3}\tau^{[n]}_{ll}\delta_{ik} = \tau^{[n]}_{ik} + \frac{2}{3}K^{[n]}\delta_{ik}$, and $\nu^{(n)}$ is the *turbulent viscosity* of the fluid at the length scale Δ_n. Since viscosity can be expressed as the product of a length scale and a characteristic velocity, a customary hypothesis identifies $\nu^{(n)} = C^{(n)}_\nu \Delta_n \sqrt{k^{[n]}}$. Hence,

$$\Pi^{(n)} - \frac{2}{3}k^{[n]}d^{[n]} \mathrel{\overset{\circ}{=}} \rho^{(n)} C^{(n)}_\nu \Delta_n \sqrt{k^{[n]}} |S^{*\,[n]}|^2. \tag{4.3}$$

If turbulence were self-similar within a certain range of length scales, then one would expect $C^{(n)}_\nu$ to be scale invariant, when it was averaged over appropriate regions of the flow. In order to test this proposition *a priori*, we filtered simulation data in the intermediate range of scales between the grid resolution and the integral scale. For the explicit evaluation of the turbulence stress tensor, an *enhanced viscosity approximation* was applied. This means that the ideal velocity field in definition (3.9) is replaced by the numerically computed field, which is smooth on scales $l \lesssim \Delta$ due to numerical discretisation. Equivalently, one can think of the smoothness being caused by an associated numerical viscosity, which enhances the physical viscosity of the fluid. By the same line of reasoning as in the case of two filters with $\Delta_n \gg \Delta_m$, it follows that $\langle \overset{\infty}{q} \rangle_n \simeq \langle \langle \overset{\infty}{q} \rangle_{\text{eff}} \rangle_n = \langle q \rangle_n$ if $\Delta_n \gg \Delta_{\text{eff}}$. Moreover, $\exists N : \Delta_{N+1} < \Delta_{\text{eff}} \leq \Delta_N$. According to the asymptotic equation (3.13), $\tau^{[n]}_{ik}$ can be approximated by $\tau^{[N,n]}_{ik}$. This, in turn, implies

$$\tau^{[n]}_{ik} \simeq -\langle \rho v_i v_k \rangle_n + \rho^{(n)} v^{[n]}_i v^{[n]}_k \tag{4.4}$$

for a filter of significantly larger characteristic length than the the numerical scale Δ_{eff}. Here v_i is the PPM solution of the quasi-Euler equation (2.2).

However, the actual range of inertial scales in the case of the simulation discussed in §2 is rather marginal. From the turbulence energy spectrum shown in figure 1, one can see that approximate Kolmogorov scaling is found for dimensionless wave numbers in the narrow range $2 \lessapprox \tilde{k} \lessapprox 5$. The dimensionless wave number associated with a Gaussian filter of characteristic length scale Δ_n is $\tilde{k}_n = (\pi/\Delta_n)(L/2\pi) = L/2\Delta_n$. Thus, only filters with $0.1 \lessapprox \Delta_n/L \lessapprox 0.25$ are more or less suitable for calculating $C^{(n)}_\nu$ from (4.3), if the the turbulence stress tensor is substituted by the enhanced viscosity approximation (4.4). Notwithstanding these tight constraints, mean values of $C^{(n)}_\nu$ were calculated from a sample of data sets using several different filters. The results are plotted as functions of the characteristic filter wave number in figure 2. Although, as a consequence of the rather limited resolution of the simulations, pronounced self-similarity is not apparent, basic trends can be discerned. In the case of purely subsonic turbulence with the characteristic Mach number $V/c_0 \approx 0.084$, the plotted values seem to indicate a maximum of $\langle C^{(n)}_\nu \rangle$ near the wave number $\tilde{k} = 2.0$, which marks the upper bound of the energy-containing subrange. Towards higher wave numbers, i. e., for filters of smaller characteristic length, $\langle C^{(n)}_\nu \rangle$ decreases and eventually flattens in the vicinity of maximum dissipation at the wave number $\tilde{k}_{\text{p}} \approx 13.5$. For the other simulations, a similar behaviour emerges, but there is seemingly a trend toward smaller production parameters for increasing Mach number and partially dilatational forcing. In any case, we suggest to adopt $\langle C_\nu \rangle \approx 0.06$ as a good value for fully developed turbulence. This choice is further supported by the selection of numerical values listed in table 2, which were obtained with the particular filter of characteristic wave number $\tilde{k}_6 = 3$. Near this wave number, the compensated energy spectra exhibit local minima.

A different notion of self-similarity originates from the correlation of turbulence stresses modelled upon the eddy-viscosity closure in consecutive bands of wave numbers. Actually, so-called dynamical procedures for the computation of subgrid-scale closure param-

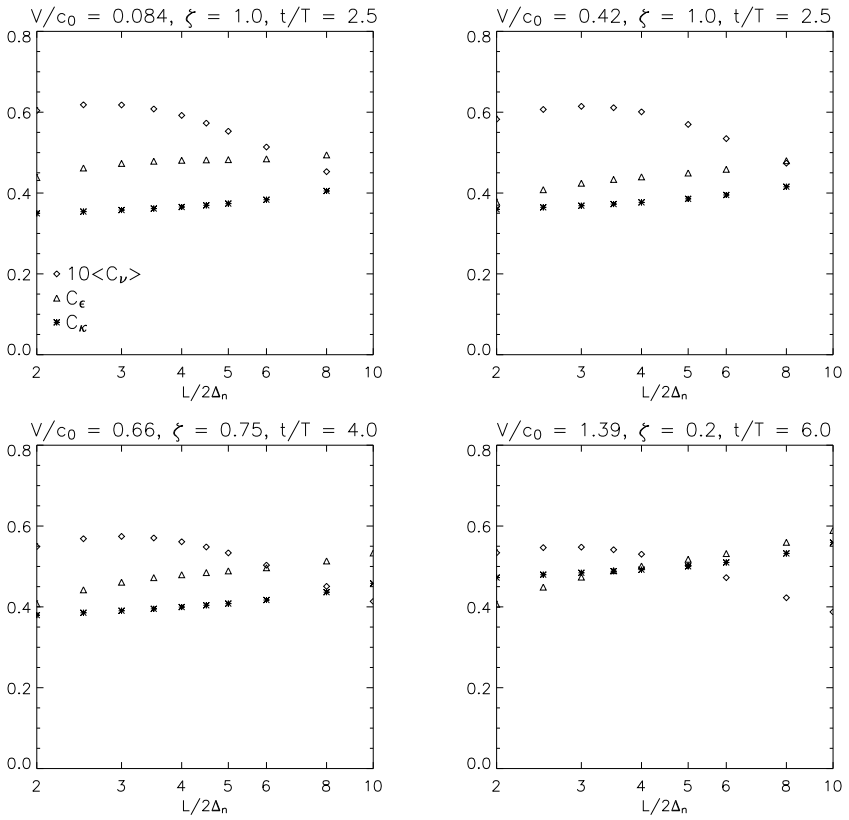

FIGURE 2. Numerically evaluated closure parameters $\langle C_\nu \rangle$, C_ϵ and C_κ as functions of the normalised wave number $\tilde{k}_n = L/2\Delta_n$ for Gaussian filters of characteristic length Δ_n.

V/c_0	ζ	t/T	$\langle C_\nu^{(6)} \rangle$	$C_\epsilon^{(6)}$	$C_\kappa^{(6)}$
0.084	1.0	2.5	0.0618	0.473	0.358
0.42	1.0	2.5	0.0615	0.424	0.369
0.66	0.75	4.0	0.0574	0.461	0.390
1.39	0.20	6.0	0.0548	0.474	0.484

TABLE 2. Mean production, dissipation and diffusion parameters calculated with a Gaussian filter of characteristic length $\Delta_6 = L/6 = 24\Delta$. The values in the first three columns specify the characteristic Mach number V/c_0, the spectral weight ζ of the driving force and the instant of time t/T for the chosen data sets extracted from different numerical simulations.

eters, in particular, C_ν, make use of this kind of similarity. Originally, dynamical formulations of the well-known Smagorinsky model and the SGS turbulence energy equation model utilised the proposition that turbulence stresses at different filter levels are similar (see Germano, Piomelli, Moin & Cabot, 1991; Erlebacher, Hussaini, Speziale & Zang, 1992; Piomelli & Liu, 1995; Meneveau & Katz, 2000). The ratio of the filter length scales in this approach is usually set equal to a factor of two. Thus, using the notation introduced in §3, the similarity hypothesis amounts to $C^{(n)} = \langle C^{(2n)} \rangle_n$. Contrary to the statistical scale invariance of $C^{(n)}$ investigated earlier in this section, this is a *local* relation, which presumes significant correlation between the turbulence stresses $\tau_{ik}^{(n)}$ and $\langle \tau_{ik}^{(2n)} \rangle_n$.

On the other hand, Liu, Meneveau & Katz (1994) found evidence for a more pronounced correlation between $\tau_{ik}^{(2n)}$ and the intermediate stress tensor $\tau_{ik}^{[2n,n]}$. The latter is also known as the Leonard's stress tensor in the context of SGS models. They processed data obtained from velocity measurements in round jet experiments with filters of varying characteristic length scale in order to evaluate the turbulence stresses and the rate of energy transfer across certain wave numbers. Making use of the data produced in our numerical simulations, we re-investigated the relation reported by Liu *et al.* (1994). To this end, the function $C_\nu^{(2n,n)}(\boldsymbol{x},t)$ was determined from the intermediated stress tensor $\tau_{ik}^{[2n,n]}$ associated with the range of scales $\Delta_{2n} \lessapprox l \lessapprox \Delta_n = 2\Delta_{2n}$:

$$C_\nu^{(2n,n)} = \frac{\tau^{*\,[2n,n]}(v_i^{[2n]}, v_k^{[2n]}) S_{ik}^{[n]}}{\rho^{(n)} \Delta_n \sqrt{k^{[2n,n]}} |S^{*\,[n]}|^2} \tag{4.5}$$

The quantities in the above expression can be evaluated by filtering the data at two levels n and $2n$, in between the energy containing and the dissipation range. The *similarity closure* for the turbulence stress $\tau_{ik}^{[2n]}$ associated with the length scale Δ_{2n} is then given by

$$\tau_{ik}^{*\,[2n]} S_{ik}^{[2n]} \triangleq C_\nu^{(2n,n)} \rho^{(2n)} \Delta_{2n} \sqrt{k^{[2n]}} |S^{*\,[2n]}|^2. \tag{4.6}$$

In order to validate the modelled rate of production according to (4.6), once more the turbulence stress tensor on the left-hand side was evaluated by means of the enhanced viscosity approximation.

The deviations of both the statistical and the similarity closure from the explicitly evaluated rate of turbulence energy production is illustrated in figure 3. First of all, figure 3 (a) shows a contour plot of $\tau^{*\,[6]} S_{ik}^{[6]}$, which was computed with a Gaussian filter of characteristic length $\Delta_6 = L/6$ from a 2D section of the flow in the simulation with purely solenoidal forcing and characteristic Mach number $V/c_0 \approx 0.42$ at time $\tilde{t} = 2.5$. The corresponding turbulent-viscosity closure with the production parameter set equal to $\langle C_\nu^{(6)} \rangle \approx 0.0615$ is plotted in figure 3 (c). Although the overall agreement is satisfactory, regions of pronounced production are evidently not reproduced. On the other hand, the similarity parameter $C_\nu^{(6,3)}$ was computed from (4.5). The corresponding contour plot is shown in figure 3 (b). Obviously, $C_\nu^{(6,3)}$ is negative in several regions of the flow. The resulting negative turbulent viscosity is usually interpreted as *backscattering* of energy from smaller to larger scales (see Sagaut, 2001, §4.4). In fact, energy transfer upwards through the cascade is well known from turbulence theory and can be accounted for by localised closures. The outcome of inserting $C_\nu^{(6,3)}$ into the turbulent-viscosity closure for $\tau^{*\,[6]} S_{ik}^{[6]}$ is shown in figure 3 (d). The deviations from explicitly evaluated rate of production are clearly less than in the case of the closure with the constant statistical parameter. Although some residual errors persist, the localised closure performs much better in regions of large turbulence stresses. Moreover, it gives a fair approximation to backscattering.

5. The rate of dissipation

The rate of dissipation at the level of the n-th filter,

$$\epsilon^{(n)} = \nu \langle |\overset{\infty}{S^*}|^2 \rangle_n, \tag{5.1}$$

specifies the rate of conversion of kinetic energy into internal energy due to microscopic viscous dissipation. The filter operation corresponds to local averaging of the rate of

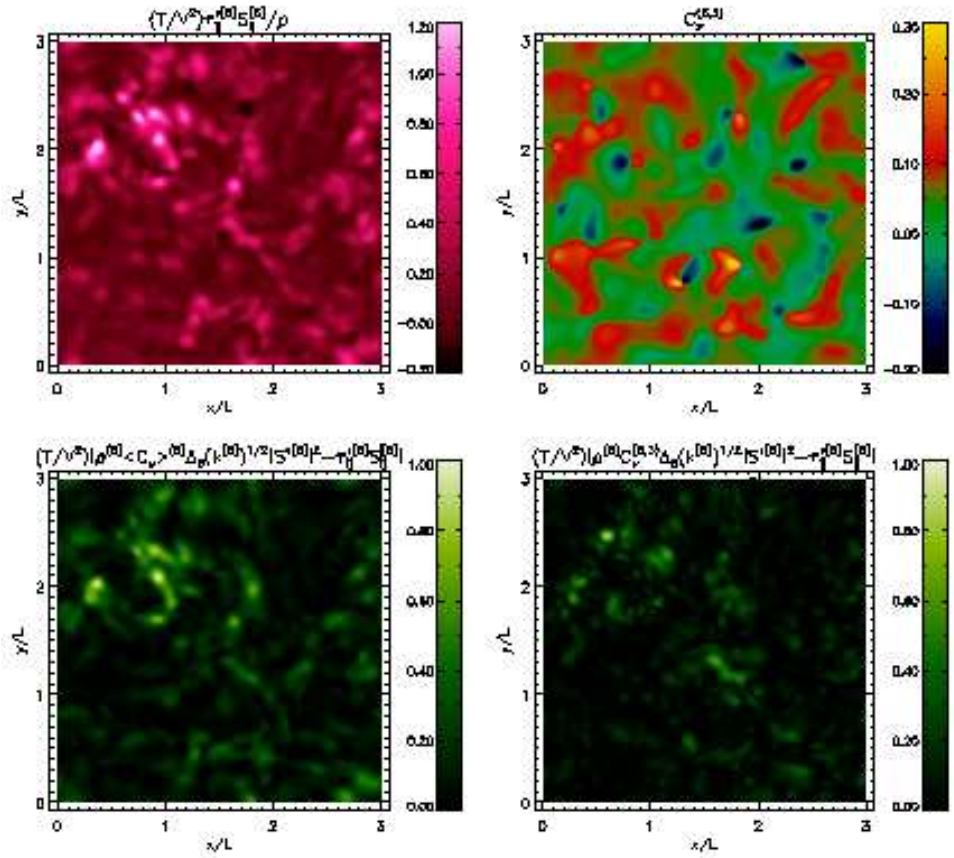

FIGURE 3. The rate of turbulence production evaluated from filtered data of the simulation with purely solenoidal forcing and $V/c_0 \approx 0.42$ in the plane $z = 0$ at time $\tilde{t} = 2.5$ (a: left top panel) and the corresponding deviations of the statistical and the localised turbulent-viscosity closure, respectively (c, d: bottom panels). Also shown is the localised production parameter inferred from a similarity hypothesis (b: right top panel).

dissipation over length scales $l < \Delta_n$. Regardless of the filter length Δ_n, the rate of dissipation $\epsilon^{(n)}$ is largely determined by velocity fluctuations on the smallest dynamical scales near the microscopic Kolmogorov length $\eta_{\rm K}$. For this reason, there is no way of explicitly evaluating $\epsilon^{(n)}$ from under-resolved numerical data. A simple estimate can be made if the resolved flow is more or less in stochastic equilibrium. Taking the global average of the turbulence energy equation (3.17), the diffusion term cancels out, and the mean time derivative is negligible in the case of steady turbulence. Hence,

$$\left\langle \frac{1}{\rho^{(n)}} \Pi^{(n)} \right\rangle \simeq \langle \epsilon^{(n)} + \lambda^{[n]} \rangle. \tag{5.2}$$

The contribution $\lambda^{(n)}$ stems from pressure dilatation:

$$\rho^{(n)} \lambda^{[n]} \equiv -\langle \overset{\infty}{P} \overset{\infty}{d} \rangle_n + P^{(n)} d^{[n]}. \tag{5.3}$$

Equation (5.2) expresses the well known equilibrium hypothesis for the balance between turbulence production and dissipation in the quasi-stationary regime for the dynamics on length scales $l \gtrsim \Delta_n$. The validity of this hypothesis has recently been confirmed for

incompressible turbulence by directly computing the spectral energy transfer function from numerical data (see Kaneda, Ishihara, Yokokawa, Itakura & Uno, 2003).

The most common closure for the rate of dissipation is the dimensional expression

$$\epsilon^{(n)} \triangleq C_\epsilon^{(n)} \frac{\left\langle \left(k^{[n]}\right)^{3/2} \right\rangle}{\Delta_n}. \tag{5.4}$$

In general, the parameter $C_\epsilon^{(n)}$ varies in space and time. However, in the case of statistically stationary homogeneous turbulence, the closure hypothesis can be simplified further by assuming a constant value of $C_\epsilon^{(n)}$. In order to fulfil statistical equilibrium, we therefore set

$$C_\epsilon^{(n)} = \frac{\Delta_n \left\langle \frac{1}{\rho^{(n)}} \Pi^{(n)} - \lambda^{[n]} \right\rangle}{\left\langle \left(k^{[n]}\right)^{3/2} \right\rangle}. \tag{5.5}$$

Results calculated from simulation data are shown in figure 2. It appears that the graphs of $C_\epsilon^{(n)}$ flatten near the transition to the range of wave numbers dominated by dissipation. In particular, for the simulations with lower Mach number, $C_\epsilon^{(8)} \approx 0.48$. Even for the higher Mach numbers, the corresponding values of the dissipation parameter are not much different. This falls in place very well with the results discussed by Kaneda *et al.* (2003). A further sample of values for the dissipation parameter is listed in table 2. In most cases, $C_\epsilon^{(n)}$ is slightly less than 0.5 for the filter levels $6 \leq n \leq 12$, which highlights the robustness of this parameter.

6. Turbulent diffusion

The turbulent flux of kinetic energy is given by

$$F_k^{[n]} = \frac{1}{2} \tau_{iik}^{[n]} + \mu_k^{(n)}, \tag{6.1}$$

where the contracted third-order moments (TOM) $\tau_{iik}^{[n]}$ and the pressure-diffusion flux $\mu^{(n)}$ are defined by

$$\tau_{iik}^{(n)} \equiv \tau(\overset{\infty}{v}_i, \overset{\infty}{v}_i, \overset{\infty}{v}_k) = -\langle \overset{\infty}{\rho} \overset{\infty}{v}_i \overset{\infty}{v}_i \overset{\infty}{v}_k \rangle_n - 2\tau_{ik}^{[n]} v_i^{[n]} + \langle \overset{\infty}{\rho} \overset{\infty}{v}_i \overset{\infty}{v}_i \rangle_n v_k, \tag{6.2}$$

and

$$\mu_k \equiv \tau(\overset{\infty}{P}, \overset{\infty}{v}_k) = -\langle \overset{\infty}{P} \overset{\infty}{v}_k \rangle_n + P^{(n)} v_k^{[n]}. \tag{6.3}$$

In the well known gradient-diffusion closure, the flux is set equal to the mean product of kinetic diffusivity and the gradient of the turbulence energy:

$$\boldsymbol{F}^{[n]} \triangleq \rho^{(n)} C_\kappa^{(n)} \Delta_n \sqrt{k^{[n]}}\, \boldsymbol{\nabla} k^{[n]}. \tag{6.4}$$

This closure immediately reveals a consistency problem. The parameter $C_\kappa^{(n)}$ is overdetermined, as there are three flux components. For a well defined solution, the gradient of $k^{[n]}$ being aligned with the flux vector $\boldsymbol{F}^{[n]}$ is an indispensable precondition. If this were the case, a least-square approach could be employed in order to calculate the closure parameter:

$$C_\kappa^{(n)} = \frac{\langle \boldsymbol{F}^{[n]} \cdot \boldsymbol{\nabla} k^{[n]} \rangle}{\langle \rho^{(n)} \Delta_n \sqrt{k^{[n]}} |\boldsymbol{\nabla} k^{[n]}|^2 \rangle}. \tag{6.5}$$

In the particular case of the simulation with partially dilatational forcing ($\zeta = 0.66$),

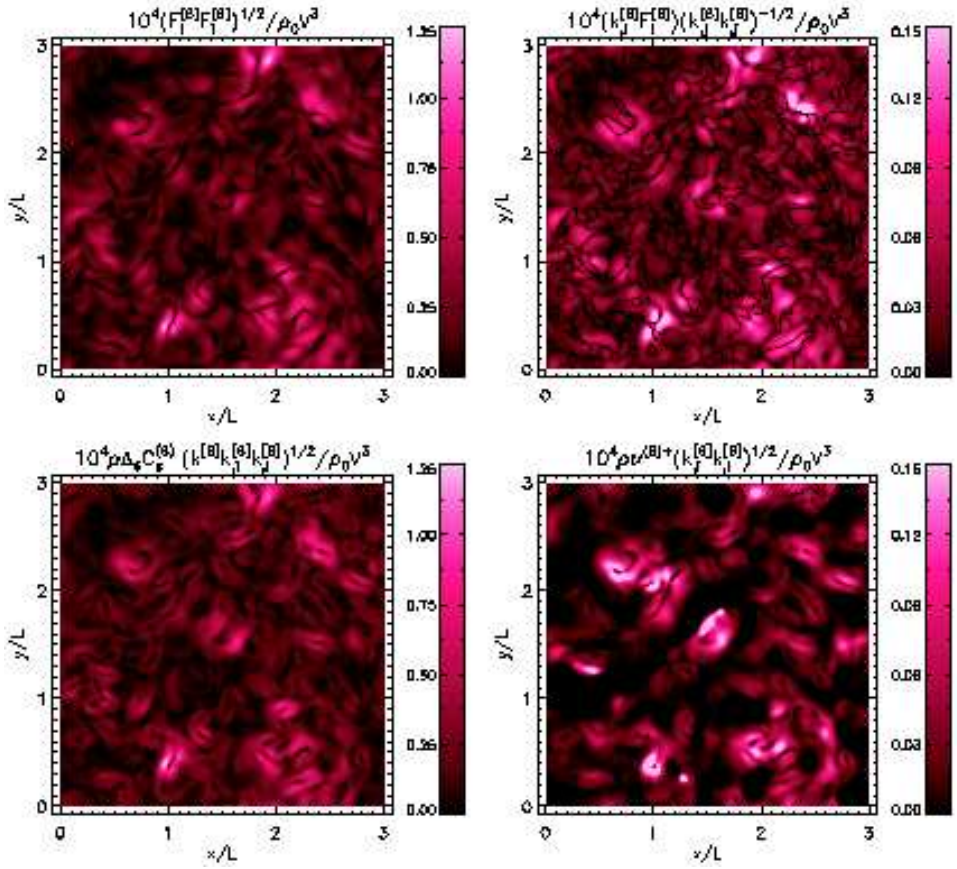

FIGURE 4. The turbulent flux magnitude computed with a Gaussian filter of characteristic length $\Delta_6 = L/6$ from data of the simulation with $\zeta = 0.75$ and $V/c_0 \approx 0.66$ at time $\tilde{t} = 5.0$. Shown are the contours of the actual flux magnitude $|\boldsymbol{F}^{[6]}|$ (a: left top panel), the projection of the modelled flux as defined by equation (6.5) unto the actual flux (b: right top panel), and contours of differently modelled fluxes (c, d: bottom panels).

the outcome of this ansatz was matched against the explicitly evaluated flux $F_k^{[6]}$ for a 2D section of the filtered flow at time $\tilde{t} = 4.0$. The filtering length is $\Delta_6 = L/6$. Equation (6.5) yields $C_\kappa^{(6)} \approx 0.0358$ from the full 3D data set, which is of the same order of magnitude as the corresponding mean parameter of production, $C_\kappa^{(6)} \approx 0.0574$. From this, a turbulent kinetic Prandtl number close to one seems to be supported. However, the overall agreement between the modelled and the explicitly evaluated turbulent flux is actually very poor, as is revealed by a comparison of the figures 4 (a) and 4 (b). The flux magnitude is underestimated by almost a decade, according to the different scales of either plots. This discrepancy definitely indicates that the *a priori* assumption of turbulent transport in the direction of the turbulence energy gradient is not fulfilled. In particular, those points where the turbulence energy gradient is oriented nearly perpendicular to the turbulent flux vector appear as dark wiggling ribbons in figure 4 (b).

In consequence, we forsook the approach outlined so far and determined the diffusivity

parameter by matching the flux magnitudes rather than the flux vectors:

$$C_\kappa^{(n)} = \frac{\langle |\boldsymbol{F}^{[n]}| \rangle}{\langle \rho^{(n)} \Delta_n \sqrt{k^{[n]}} |\boldsymbol{\nabla} k^{[n]}| \rangle}. \tag{6.6}$$

Implementing this equation, $C_\kappa^{(6)} \approx 0.390$ was obtained from the aforementioned simulation data. In fact, this value is larger by about an order of a magnitude than the corresponding value computed with (6.5). Contours of the corresponding modelled flux, $\rho^{(6)} C_\kappa^{(6)} \Delta_6 \sqrt{k^{[6]}} |\boldsymbol{\nabla} k^{[6]}|$, are plotted in figure 4 (c). The remarkably good correlation to $|\boldsymbol{F}^{[6]}|$ is evident. Even surfaces at which the flux vanishes, as a result of pressure-diffusion cancelling the TOM contributions, are well reproduced. Therefore, we conclude that the gradient-diffusion closure is a fair statistical description of turbulent transport, which correctly accounts for the magnitude but not for the local direction of transport. Numerically calculated values of $C_\kappa^{(6)}$ for different simulations are listed in table 2. It appears that there is a trend towards stronger diffusion for higher Mach numbers. Figure 2 shows the variation of $C_\kappa^{(n)}$ with the smoothing length scale Δ_n. As one can see, the parameter of diffusion is almost scale-invariant for $n \in 2, \ldots, 10$, which corresponds to the nearly inertial subrange.

In addition, we tested whether turbulent diffusivity is correlated with the turbulent viscosity, since $\kappa^{(n)} = \sigma_{\mathrm{kin}}^{(n)} \nu^{(n)}$ with $\sigma_{\mathrm{kin}} \sim 1$ is a commonly used hypothesis. To this end, the parameter $C_\nu^{(n)}$ was computed locally, according to the prescription in §4. Then the diffusivity was set equal to the viscosity for positive values of $C_\nu^{(n)}$. On the other hand, $C_\nu^{(n)}$ was set identically zero in regions of negative production, because concentration of turbulence energy due to negative diffusivity has to be inhibited. The numerical evaluation demonstrated that the resulting diffusive flux is typically too small by an order of a magnitude. An exemplary 2D contour section is shown in figure 4 (d). The assumption of a kinetic Prandtl number close to unity is thus clearly invalidated.

7. Conclusion

We have investigated parameters associated with the common closures for the turbulence energy budget equation, using data from direct numerical simulations of compressible isotropic turbulence driven by stochastic forcing. The statistical self-similarity of isotropic turbulence, which becomes manifest in the scale-invariance of averaged closure parameters within the inertial subrange, just begins to emerge at the resolution of 432 grid cells per dimension. Nevertheless, it was feasible to infer the estimates $\langle C_\nu \rangle \approx 0.06$, $C_\epsilon \approx 0.5$ and $C_\kappa \approx 0.4$ for the parameters of turbulence production, dissipation and diffusion, respectively. These estimates appear to be robust for Mach numbers $\lesssim 1$ and predominantly solenoidal forcing. Significant deviations from these values are likely to emerge from supersonic turbulence, although we are not able to make definite statements on the basis of our data. Whereas the results for the parameters of production and dissipation, respectively, agree well with various values cited in the literature, we propose a substantially enhanced parameter of diffusion. The would-be smallness of C_κ, as given by the standard hypothesis $C_\kappa \approx C_\nu$, can be attributed to the mismatch arising from the usually presumed vector alignment in the gradient-diffusion closure. We emphasise that there is no *a priori* reason for any tight relationship between the turbulence viscosity (specifying the quasi-local transport of energy from larger to smaller scales) and the turbulence diffusivity (specifying the non-local redistribution of energy on the smaller scales).

Furthermore, we compared the modelled turbulence stresses for a localised eddy-viscosity closure to the explicitly evaluated stresses and found improved correlation, in contrast to the the closure with a constant statistical parameter. This result supports the validity of dynamical procedures for the computation of C_ν in SGS models, especially, when applying the subgrid scale model proposed by Kim, Menon & Mongia (1999).

For a more stringent analysis of the self-similar regime in numerical simulations, significantly higher resolution is called for. Indeed, extremely high-resolution data have been computed recently (see Kaneda *et al.*, 2003). These data could be exploited for the evaluation of structural properties over a wide range of length scales by means of filtering.

8. Acknowledgements

Our implementation of the PPM originated from Fryxell, Müller & Arnett (1989) and was later adopted in a new code featuring MPI for massively parallel computation on high-end platforms (see Reinecke, 2001) . The turbulence simulations were run on the Hitachi SR-8000 supercomputer of the *Leibniz Computing Centre* in Munich, using 512 processors in parallel. Special thanks goes to M. Reinecke for unfailing technical advice. For the post-processing of the data, in particular, the Gaussian filtering, the *FFTW* implementation of the the fast Fourier transform algorithm was utilised (cf. Frigo & Johnson, 1998). Due to the extraordinary memory requirements, the computation of the parameters discussed in this paper was performed on a shared-memory node of the IBM p690 supercomputer of the *Computing Centre of the Max-Planck-Society* in Garching, Germany. One of the authors (W. Schmidt) was supported by the priority research program *Analysis and Numerics for Conservation Laws* of the Deutsche Forschungsgesellschaft.

References

Colella, P. & Woodward, P. R. 1984 The piecewise parabolic method (PPM) for gas-dynamical simulations. *J. Comp. Physics* **54**, 174–201.

Dobler, W., Haugen, N. E., Yousef, T. A. & Brandenburg, A. 2003 Bottleneck effect in three-dimensional turbulence simulations. *Phys. Rev. E* **68** (2), 026304–+.

Erlebacher, G., Hussaini, M. Y., Speziale, C. G. & Zang, T. A. 1992 Toward the large-eddy simulation of compressible turbulent flows. *J. Fluid Mech.* **238**, 155.

Eswaran, V. & Pope, S. B. 1988 An examination of forcing in direct numerical simulations of turbulence. *J. Comp. Physics* **16** (3), 257–278.

Frigo, M. & Johnson, S. G. 1998 FFTW: An Adaptive Software Architecture for the FFT. In *ICASSP conference proceedings*, , vol. 3, pp. 1381–1384.

Fryxell, B. A., Müller, E. & Arnett, W. D. 1989 MPA preprint 449.

Germano, M. 1992 Turbulence: the filtering approach. *J. Fluid Mech.* **238**, 325–336.

Germano, M., Piomelli, U., Moin, P. & Cabot, W. H. 1991 A dynamic subgrid-scale eddy viscosity model. *Phys. Fluids* **3**, 1760–1765.

Hillebrandt, W. & Niemeyer, J. C. 2000 Type Ia supernova explosion models. *Ann. Rev. Astron. Astrophys.* **38**, 191.

Kaneda, Y., Ishihara, T., Yokokawa, M., Itakura, K. & Uno, A. 2003 Energy dissipation rate and energy spectrum in high resolution direct numerical simulations of turbulence in a periodic box. *Physics of Fluids* **15**, L21–L24.

Kim, W., Menon, S. & Mongia, H. C. 1999 Large-Eddy Simulation of a Gas Turbine Combustor Flow. *Combust. Sci. and Tech.* **143**, 25–62.

Liu, S., Meneveau, C. & Katz, J. 1994 On the properties of similarity subgrid-scale models as deduced from measurements in a turbulent jet. *J. Fluid Mech.* **275**, 83–119.

Meneveau, C. & Katz, J. 2000 Scale-Invariance and Turbulence Models for Large-Eddy Simulation. *Annual Review of Fluid Mechanics* **32**, 1–32.

Piomelli, U. & Liu, J. 1995 Large-eddy simulation of rotating channel flows using a localized dynamic model. *Phys. Fluids* **7** (4), 839.

Pope, S. B. 2000 *Turbulent Flows*. Cambridge University Press.

Reinecke, M. A. 2001 Modeling and simulation of turbulent combustion in type Ia supernovae. PhD thesis, Technical University of Munich, Physics Department.

Sagaut, P. 2001 *Large Eddy Simulation for Incompressible Flows*. Springer.

Sytine, I. V., Porter, D. H., Woodward, P. R., Hodson, S. W. & Winkler, K. 2000 Convergence Tests for the Piecewise Parabolic Method and Navier-Stokes Solutions for Homogeneous Compressible Turbulence. *Journal of Computational Physics* **158**, 225–238.

Yeung, P. K. & Zhou, Y. 19 Universality of the Kolmogorov constant in numerical simulations of turbulence. *Phys. Rev. E* **56**, 1746–1752.